



Synthesis, characterization and photocatalytic properties of $\text{Bi}_{0.85-x}\text{M}_x\text{Ba}_{0.15}\text{FeO}_3$ (M = Na and K, X = 0, 0.1) perovskite-like nanoparticles using the sol-gel method

A. Haruna*, I. Abdulkadir, S.O. Idris

Department of Chemistry, Ahmadu Bello University, Zaria-Nigeria

ARTICLE INFO

Article history:

Received 12 March 2019

Revised 22 April 2019

Accepted 19 May 2019

Available online 20 May 2019

Keywords:

Sol-gel method

Photocatalyst

Metal doping

Nanoparticles

ABSTRACT

Bismuth barium ferrite $\text{Bi}_{0.85-x}\text{M}_x\text{Ba}_{0.15}\text{FeO}_3$ (M = Na and K, x = 0, 0.1) nanoparticles doped with sodium and potassium metal ions were synthesized via the citric acid ($4.0 \times 10^{-1} \text{ moldm}^{-3}$) route in the presence of sodium dodecyl sulfate, SDS (0.35 moldm^{-3}) by sol-gel method. The obtained powders were pre-calcined at 400°C for 4 h. Separate portions each of the powders were annealed at temperatures of 600, 700 and 800°C for 4 h. The powders were characterized using the X-ray diffraction (XRD) method, which indicated that the powders have a perovskite structure which have crystallized in rhombohedral lattice. Scanning electron microscopy (SEM) images showed clusters of polycrystalline nanoparticles having uniform sizes. Fourier Transform Infra-red (FTIR) spectrophotometer was used to investigate the B-site formation and purity of the perovskite nanoparticle. The Uv-vis DRS spectrum of the powders was also determined. The performance of the powder as photocatalyst was evaluated using a model organic pollutant, Methylene blue, under visible light irradiation for 2 h. The Na and K doped powders showed a very useful application for photodegradation of the dye under the visible light region. Studies in this research showed that powders annealed at 400°C were not very active and that activity increased with increased in annealing temperature. The photocatalytic activities of the powders is enhanced with the addition of peroxide (H_2O_2) and the effect of pH was investigated.

© 2019 The Authors. Production and hosting by Elsevier B.V. on behalf of King Saud University. This is an open access article under the CC BY-NC-ND license (<http://creativecommons.org/licenses/by-nc-nd/4.0/>).

1. Introduction

In recent times, perovskite nanomaterials have been found to show very interesting and fascinating multifunctional properties suitable for numerous applications (Abdulkadir et al., 2016; Kanhere and Chen, 2014). The increasing focus on these functional oxides has revealed exciting properties with potentials for application in multiferroic materials (Vasala and Karppinen, 2014). The

Abbreviations: BFO, Bismuth ferrite; BBFO, Bismuth barium ferrite; KBFO, Potassium doped bismuth barium ferrite; NBFO, Sodium doped bismuth barium ferrite; MB, Methylene blue; MO, Methyl orange; RhB, Rhodamine B; SDS, Sodium dodecyl sulfate; PXRD, Powder X-ray Diffraction.

* Corresponding author.

E-mail address: abdurashid.haruna@yahoo.com (A. Haruna).

Peer review under responsibility of King Saud University.



<https://doi.org/10.1016/j.jksus.2019.05.005>

1018-3647/© 2019 The Authors. Production and hosting by Elsevier B.V. on behalf of King Saud University.

This is an open access article under the CC BY-NC-ND license (<http://creativecommons.org/licenses/by-nc-nd/4.0/>).

structure of perovskite materials is such that it can allow substitution and replacement of the ions on either the A- or B-site and by selecting atoms with suitable properties, novel materials with interesting properties were produced over the last few years. Doping with either divalent (Ca, Sr, Pb, Ba) or trivalent (La, Nd, Tb, Sm, Gd) metal ions helps in stabilizing the single phase structure of BiFeO_3 (BFO) giving it extra advantage (Narayan et al., 2013). Perovskite-like nanoparticles show varying physical and chemical properties and can have electrical properties ranging from insulating to metallic; they show superconductivity; they have different magnetic arrangements varying from antiferromagnetic, ferrimagnetic and ferromagnetic; they also show ionic conductivity as well as photocatalytic properties (Kim, 2016; Bismibanu, 2018). The electronic applications of BiFeO_3 (BFO) powders in addition to the photocatalytic properties were also reported under the visible-light region of electromagnetic spectrum (Kim, 2016).

Reports show that some BFO nanoparticles have been used in water experiments in visible light for generation of hydrogen by water splitting (Soltani and Entezari, 2014). BFO powders have been synthesized via various synthetic routes, namely; sol-gel,

hydrothermal, combustion and co-precipitation synthetic methods (Li et al., 2010). It is chemically stable due to its narrowing bandgap of 2.2 eV (Kim, 2016). Aside from theoretical work, considerable experimental efforts have been made to change the band structure of BiFeO₃ by doping. The photocatalytic decomposition of organic contaminants by BFO nanowires for oxygen generation was reported (Gao et al., 2015). BiFeO₃ at room temperature was described to have hexagonal [1 1 1] (Narayan et al., 2013), rhombohedral [1 1 1] (Ahmed et al., 2012) and pseudo-cubic [0 0 1] (Chen et al., 2012) nanostructure unit cells. The rhombohedral perovskite structure is stable, although it undergoes a change in structural transition at near 1098 K from orthorhombic phase to pseudo-cubic phase at 1204 K (Chen et al., 2012).

Over the last few years, the increasing use of noble metals to improve photocatalytic performance of materials is an area of interest for most researchers. BFO nanoparticle doped with metal cations have shown great promise in enhancing the photocatalytic performance of materials finding numerous applications. Photodegradation of Rhodamine B (RhB) with BiFeO₃/Bi₂Fe₄O₉ was found to be 2.7 times higher than BFO material and 2.0 times in hydrogen evolution from water splitting under visible light (Zhang et al., 2017). BFO-doped material leads to an enhanced performance in photocatalytic degradation of organic dyes; MB, MO and RhB as reported (Wang et al., 2016). In another report, pure BFO material and 50% BiVO₄ was used to form composite that gives best photocatalytic performance on photodegradation of RhB used for environmental purification (Fan et al., 2016).

In this research, Bi_{0.85-x}M_xBa_{0.15}FeO₃ (M = Na and K for x = 0, 0.1) nanoparticles were synthesized using the sol-gel route. Sol-gel method of synthesis by nature is simple, not needing too much energy (70–100 °C), is relatively cost effective, gives high yield with control size and morphology of the synthesized nanoparticle (Pandey and Misha, 2011; Pomogailo, 2005). BFO doped with Ba and Na metals were reported (Chaudhuri and Mandal, 2014; Li et al., 2010; Soltani and Lee, 2016). The effects of doping of BBFO with Na⁺ and K⁺ metal ions into the crystal lattice of BiBa_{0.15}FeO₃ (BBFO), were investigated. The effect of pH and their visible light induced properties were investigated on MB in the presence and absence of peroxide. The materials were characterized and discussed. A surfactant, Sodium dodecyl sulfate (SDS) was used in the synthesis procedure to ensure nucleation of the particles and limited growth of the crystals.

2. Experimental

2.1. Materials

Ba(NO₃)₂, Bi(NO₃)₃·5H₂O, NaOH, Fe(NO₃)₃·9H₂O, NaNO₃, KNO₃, citric acid, C₆H₈O₇·H₂O, HCl, ethylene glycol, NH₄OH (30% NH₃) and Sodium Dodecyl Sulfate (SDS). Distilled water was used throughout the experiment. Analytical grade chemicals purchased from Sigma-Aldrich Chemical Company were used for this research without further purification.

2.2. Synthesis of Bi_{0.85-x}M_xBa_{0.15}FeO₃ (x = 0, 0.1, M = Na, K)

Nanoparticles of bismuth barium ferrite doped with sodium and potassium metal ions (Bi_{1-x}M_xBa_{0.15}FeO₃, x = 0, 0.1, M = Na, K) were prepared by sol-gel method. Calculated amounts of analytical grade bismuth nitrate Bi(NO₃)₃·5H₂O, Ba(NO₃)₂, Fe(NO₃)₃·9H₂O, and of metal nitrates (NaNO₃, KNO₃), were dissolved in 100 ml distilled water. Citric acid (4.0 × 10⁻¹ moldm⁻³) to metal nitrates ratio (2:1) was added and stirred continuously for about 50 min at 90 °C. 20 cm³ of ethylene glycol as a polymerization and structure directing agent was added to the mixture under continuous

heating and stirring at 90 °C for 1 h. Sodium Dodecyl Sulfate (0.35 moldm⁻³) was added to the solution and then ammonium hydroxide (30% NH₃) was added in drops to the solution mixture and the pH was maintained at 8. A thick gel was formed after heating and stirring and the gel obtained was removed from the beaker and placed to dry in an oven at 120 °C for 6 h. In order for the organic components presents to be removed, the dried powdered nanoparticles were pre-calcined at 400 °C for 4 h. Bi_{0.85}Ba_{0.15}FeO₃, Bi_{0.75}Na_{0.1}Ba_{0.15}FeO₃, and Bi_{0.75}K_{0.1}Ba_{0.15}FeO₃ all in pure phases were formed. Muffle furnace at the rate of 1 °C/min was used to subsequently annealed separate sample portions of the powders 600, 700 and 800 °C for 4 h.

2.3. Characterization

PerkinElmer Spectrum 100 FTIR spectrometer was used to collect the spectra of all powders. Scanning Electron Microscopy (SEM) images of the powdered nanoparticles were investigated using the JEOL/EO Version 1.0 (JSM-6610). The scanning was performed between 10 and 80° 2θ with a scanning speed of 3°/min at 40 kV and 40 mA. Powder X-ray diffraction (PXRD) pattern of the powders prepared under different conditions were measured using the Cu Kα (λ = 1.5406 Å) on a Rigaku Ultima IV X-ray diffractometer. UV-Vis spectrophotometer (Agilent technology, Cary Series) was used throughout in the absorbance measurement.

2.4. Photocatalytic performance

Methylene blue was used as the model organic pollutants in this photocatalytic reaction to determine the photodegradation efficiency of the perovskites BBFO, NBFO and KBFO nanoparticles at temperatures of 400–800 °C. The photocatalytic reactions of the powdered nanoparticles were performed in a Continuous Stir Tank Photoreactor (CSTP) with a magnetic stirrer at 50 rpm and a 250 W (Xe lamp; λ greater than 420 nm) (Osram, Germany) placed few centimeters above the beaker. A 10 mg/L MB concentration was prepared and determined using UV-vis spectrophotometer at approximately λ_{max} = 664 nm with a catalyst loading of 15 mg. 100 ml of the dye solution adjusted at natural pH 7 was continuously stirred in magnetic stirrer for 2 h at 20 min interval for each sample in the absence of visible light. After every 20 min, 10 ml of the solution was taken for absorbance measurement. This procedure was repeated under visible lights with catalyst for the same periods until all data were gathered. The effect of few drops of H₂O₂ (1.0 moldm⁻³) on MB and with catalyst was determined.

3. Results and discussions

A black powder was obtained for all samples calcined at 400 °C and fine brown powders for samples annealed at 600 °C, 700 °C and 800 °C. The samples were coded BBFO, NBFO and KBFO accompanied by the annealing temperature such as (e.g. BBFO 400, NBFO 600 and KBFO 800 for sample powders at temperatures of 600, 700 and 800 °C respectively).

3.1. PXRD pattern of M_xBi_{0.85-x}Ba_{0.15}FeO₃

The powder x-ray diffraction peaks of the Bi_{0.85}Ba_{0.15}FeO₃ (BBFO) perovskite-like nanoparticle displays high crystallinity with minor impurity. Fig. 1 shows the beginning of the formation of peaks indicating nucleation and growth of crystals at temperature of 400 °C (Abdulkadir et al., 2016). Other emanating peaks of the composed powder at this temperature indicate the formation of mixed oxide at this initial stage. The obvious peaks of the nanoparticle indicate a distorted rhombohedral structure (Bhushan et al.,

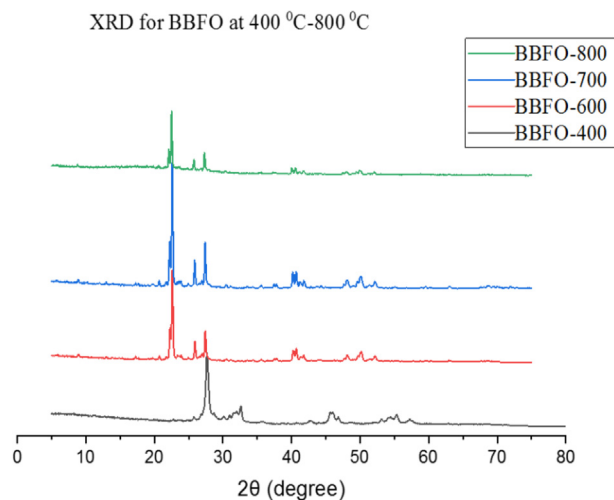


Fig. 1. PXRD peaks for $\text{Bi}_{0.85}\text{Ba}_{0.15}\text{FeO}_3$ annealed at temperatures 400–800 °C.

2009) in agreement with the structure of ceramic BiFeO_3 (Zhang et al., 2005) and different from the tetragonal structure of BiFeO_3 films as previously reported (El-Desoky et al., 2016; Yao et al., 2003). BBFO exhibit a single crystal phase with prominent peaks-splitting similar to that reported by Gao et al. (2007).

The BBFO perovskite structure belonging to R3c space group was formed. At annealing temperatures of 600 °C and above, the absence of impurity peaks and the growth of prominent peaks at higher temperatures is an indication that all the ions are well oriented into the perovskite lattices (Abdulkadir et al., 2016). In addition, at 700 °C, there is peak broadness of the powdered samples due to the higher surface area of the nanosize crystallites. However, at 800 °C, the crystals become larger with increasing peak intensities. This result agrees well with the PXRD peak intensity showing decrease in the broadness of the peaks with increasing annealing temperatures hence increase in crystallinity of the material.

Figs. 2 and 3 depict the XRD pattern of the powdered samples after doping with univalent Na^+ and K^+ metals ions. With doping, a shift in the peak was observed towards 2θ lower angles similar to that reported by (Chaudhuri and Mandal, 2014). Table 1 shows the crystallite size (average) of the materials as determined by

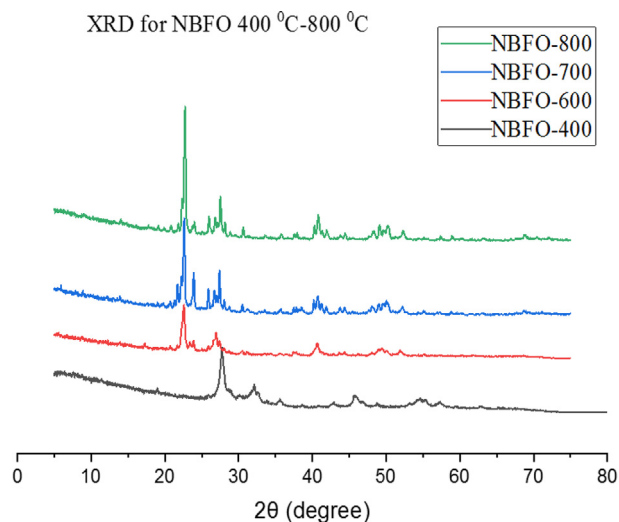


Fig. 2. PXRD peaks for $\text{Bi}_{0.75}\text{Na}_{0.1}\text{Ba}_{0.15}\text{FeO}_3$ annealed at temperatures 400–800 °C.

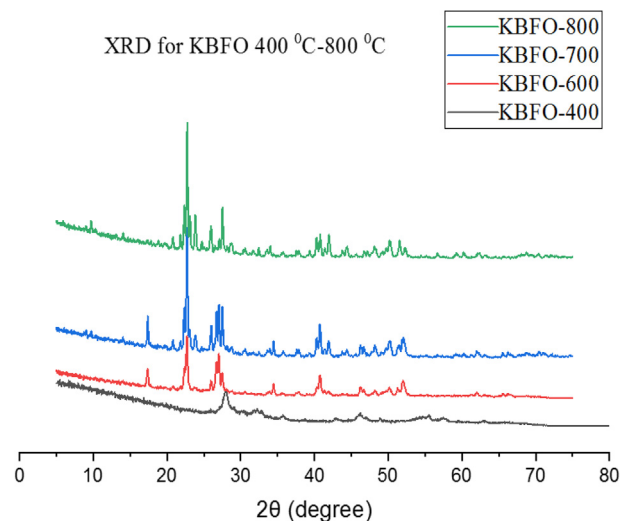


Fig. 3. PXRD peaks for $\text{Bi}_{0.75}\text{K}_{0.1}\text{Ba}_{0.15}\text{FeO}_3$ annealed at temperatures 400–800 °C.

using the Scherrer equation on the generated PXRD data. For these samples, a slight change in the average size of the crystallite of the powders was observed for the most prominent peak (1 1 0) after doping with Na and K metals. All the peaks reflection with lattice parameters $a = b = 5.576 \text{ \AA}$ and $c = 13.867 \text{ \AA}$ were easily indexed to the pure rhombohedral structure of BiFeO_3 as previously reported (Wang et al., 2012). Increasing the concentration of dopants gradually decreases the crystal size attributing it to doping ions into the BBFO lattice, inhibiting the grain growths (Wang et al., 2012). The result also shows a distortion of the lattice in the rhombohedral structure of the materials by the addition of Ba^{2+} , Na^+ and K^+ contents. This is probably due to the large ionic radius of Ba^{2+} (1.36 Å) than that of Bi^{3+} (1.17 Å) (Li et al., 2010).

3.2. ATR-FTIR spectra of perovskite like $\text{Bi}_{0.85-x}\text{M}_x\text{Ba}_{0.15}\text{FeO}_3$

Fig. 4 shows the ATR-FTIR spectra of BBFO powdered nanoparticles at temperatures of 400–800 °C indicating the formation of perovskite structure in concordance with the presented PXRD results. A broad absorbance peak in the range of $850\text{--}1350 \text{ cm}^{-1}$ is assigned to the powdered crystal as a result of adsorbed water molecule on the surface of the material. Figs. 5 and 6 shows the spectra of NBFO and KBFO respectively at 400–800 °C in the range of $500\text{--}4000 \text{ cm}^{-1}$. A stretching and bending vibrations at around 600 cm^{-1} of the perovskite material may as well suggest the formation of metal-oxygen bonds; O–Fe–O and Fe–O in the perovskite structure (Silva et al., 2010). And at lower wave numbers, decrease in peaks suggest that more of the oxides are incorporated into the perovskite structure. This result confirms the formation of B-site cation in the synthesis of the perovskite nanomaterial.

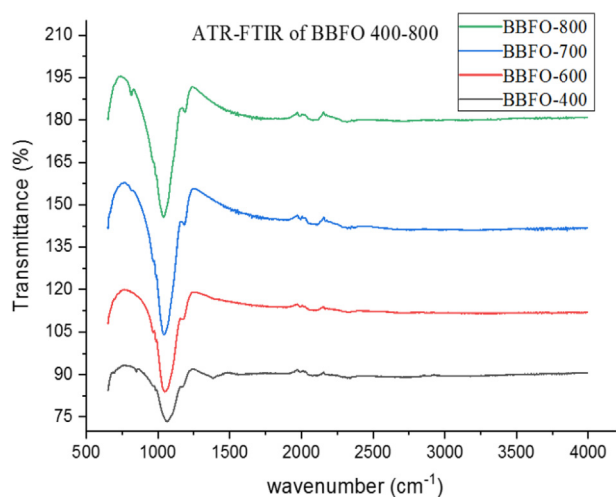
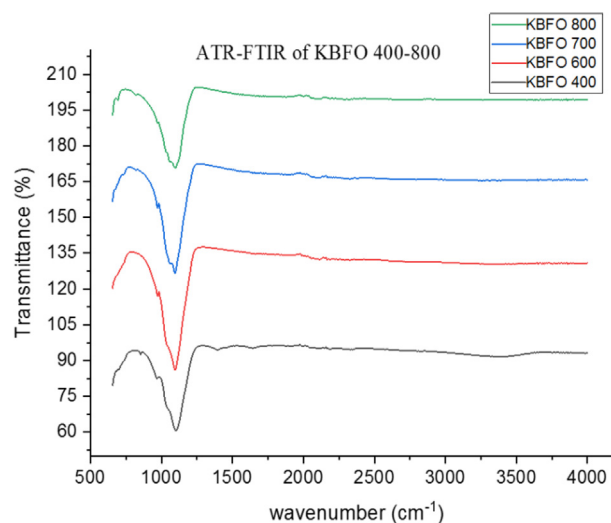
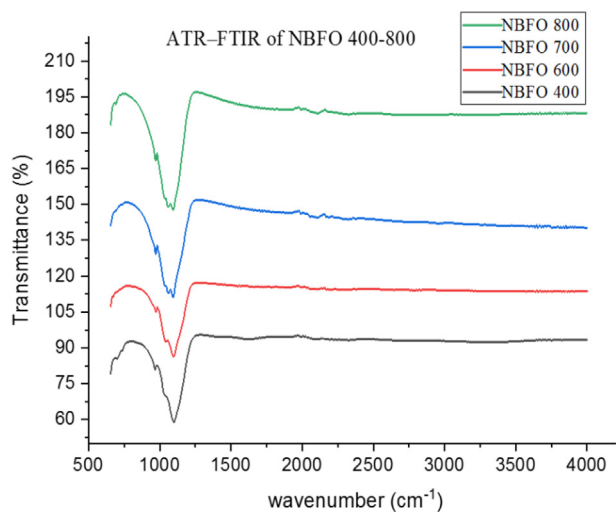
3.3. SEM images of the nanoparticle $\text{Bi}_{0.85-x}\text{M}_x\text{Ba}_{0.15}\text{FeO}_3$

Figs. 7–9 showed typical SEM images of $\text{Bi}_{0.85-x}\text{M}_x\text{Ba}_{0.15}\text{FeO}_3$ prepared by the sol-gel method. Particle size investigation of the powdered BBFO materials was performed between the annealing temperatures of 400–800 °C. A polycrystalline nanoparticle was formed at 400 °C, indicating that the perovskite nanoparticle is in uniform phase. The size of the particles is seen clearly to be uniform as the calcination temperature increases from 600 to 800 °C. There is a significant change in the shape and size of the primary particles as annealing temperature increases, the particles were seen to have a good surface area. By the doping of univalent Na^+ and K^+ metal ions, no significant difference was observed in the

Table 1

Comparison of the crystallite sizes and lattice parameters of doped and undoped BBFO at 800 °C.

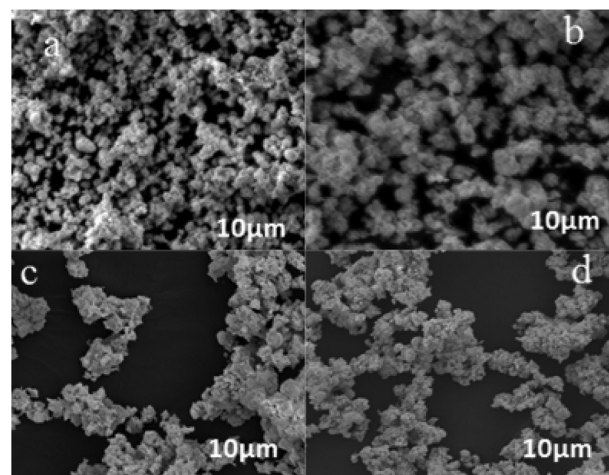
Samples	Space group	Cell parameters			Crystallite size (nm)
		a (Å)	b (Å)	c (Å)	
BBFO	R3C	5.568	5.568	13.567	32.42 ± 2
NBFO	R3C	5.571	5.571	13.552	31.16 ± 2
KBFO	R3C	5.578	5.578	13.542	28.12 ± 2

**Fig. 4.** ATR-FTIR for $\text{Bi}_{0.85}\text{Ba}_{0.15}\text{FeO}_3$ annealed at temperatures 400–800 °C.**Fig. 6.** ATR-FTIR for $\text{Bi}_{0.75}\text{Ka}_{0.1}\text{Ba}_{0.15}\text{FeO}_3$ annealed at temperatures 400–800 °C.**Fig. 5.** ATR-FTIR for $\text{Bi}_{0.75}\text{Na}_{0.1}\text{Ba}_{0.15}\text{FeO}_3$ annealed at temperatures 400–800 °C.

size of the particles having a similar particle size and particulate morphologies. These results obtained in the study is also in conformity with the XRD measurements pertaining to the uniform particle size and structure of the prepared nanoparticle.

3.4. Photocatalytic performance

The photocatalytic activity of un-doped BBFO nanoparticles for MB degradation at room temperature is depicted in Fig. 10. MB was stable in dark and under visible light irradiation when no catalyst involved. For 2 h of visible light irradiation without the BBFO nanoparticles, the degradation rate was only about 3%. Powders annealed at 400 °C were not very active, but those at 600 °C and 700 °C showed remarkable photocatalytic efficiency and better

**Fig. 7.** SEM images of (a) BBFO at 400 showing the beginning of formation of crystals, (b) A well cleared crystal showing at 600, (c) Nanospherical particles well formed (d) Dense and large crystals well-formed.

degradation efficiency was observed for powder at 800 °C. It was found to decolorize more than 65% MB dye solution after 120 min. Fig. 11a shows doping effects with Na^+ ions (NBFO) in absence of H_2O_2 , an increased photocatalytic performance of the material was observed. Fig. 12a show doping with K^+ (KBFO) after visible lights irradiation for 2 h, the degradation rate (C/C_0) of the samples were found to be below 0.3.

It will then be suggested that photocatalytic activity strongly depends on the amount of metal doping and to some extent the morphology of the particle. For the same reason, K metal doping in Fig. 12a also gives improved photocatalytic performance and in each case, powders annealed at 800 °C were found to be more

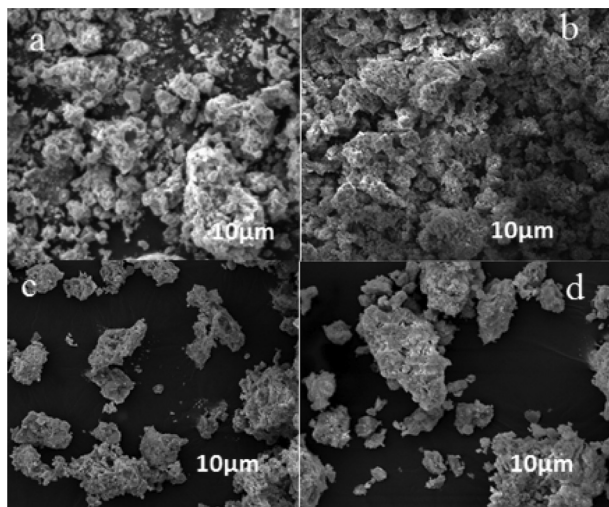


Fig. 8. SEM images of NBFO nanoparticles prepared at 400–800 °C.

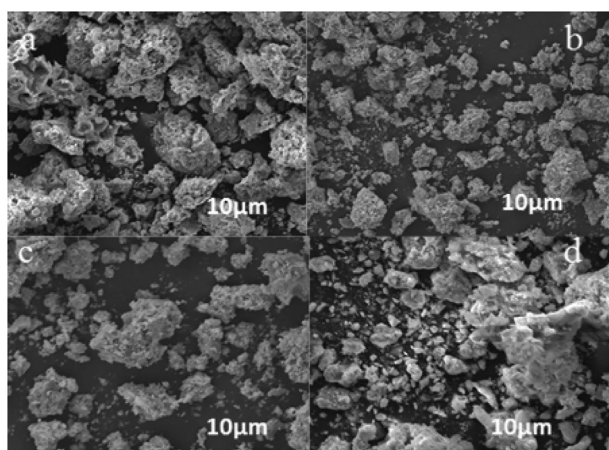


Fig. 9. SEM images of KBFO nanoparticles prepared at 400–800 °C.

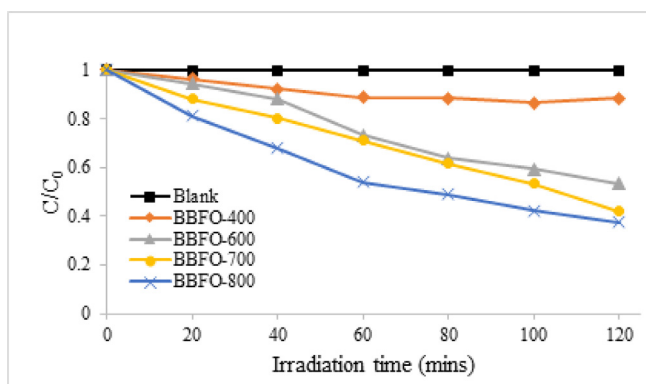


Fig. 10. Photocatalytic degradation of MB dye solution using the perovskite nanoparticle, BBFO, at different annealing temperatures of 400, 600, 700 and 800 °C.

active. NBFO and KBFO show higher photocatalytic activity than BBFO nanoparticles implying that the amount of metal (Na and K) dopants, as well as morphology plays an important role in the activity of the powders.

Rhodamine B (RhB) was degraded efficiently after 1 h to almost 4 times the photocatalytic activity of the BFO bulk material when

BiFeO₃ nanoparticle doped with Ba having an average particle size of 35 nm (Wang et al., 2011). Similar experiment was performed to effectively degrade BiFeO₃ catalyst on MB after 2 h of visible-light irradiation bringing the rate of degradation to decrease below 0.2 (Wang et al., 2012). In another study, BFO nanoparticle doped with Ca was also used to degrade Congo red in visible light irradiation, although the degradation effect was not so good (Kanhere and Chen, 2014; Zhao et al., 2014). It is very important to carry out further studies on photocatalytic activity of BFO and BBFO related materials as well as finding other application as in solid oxide fuel cells (SOFC).

3.5. Uv–vis DRS spectrum

Fig. 13 shows the Uv–visible DRS spectrum of the BBFO, KBFO and NBFO samples. The optical absorption of the samples show a strong photoabsorption property in the visible light region of electromagnetic spectrum. The corresponding band gap energy is estimated by extrapolating the linear portion of a plot of $(\alpha h\nu)^2$ against $h\nu$ using the Tauc's equation (Chang et al., 1995), where α is the absorption coefficient and $h\nu$ is the photo energy. For BBFO, KBFO and NBFO, the band gap is estimated about 2.10 eV, 2.15 eV and 2.17 eV respectively. Based on the calculated energy, the results is compared with the results of previous researches (Soltani and Entezari, 2013). Thus, BBFO, NBFO and KBFO nanoparticles may have a potential application as promising visible-light photocatalyst in water treatment.

3.6. Effect of peroxide

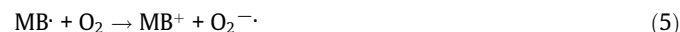
The addition of H₂O₂ greatly enhanced the photocatalytic activity of BBFO by Na⁺ and K⁺ metal ions doping. As shown in Fig. 11b, after 2 h of irradiation, the degradation rate (C/C₀) was found to be 0.2 for powders annealed at 800 °C. And at the same temperature for K⁺ metal doping, Fig. 12b also depicts that about 95% of MB was decolorized bringing the degradation rate (C/C₀) to 0.2 minimum after 2 h. The improved activity observed in Na and K metal doping, x = 0.1, could be attributed to the activation of H₂O₂ by the nanoparticles to generate hydroxyl (.OH) radicals. The MB dye in a series of reaction steps in Eqs. (1) and (2) under visible light irradiation produces a number of products; harmless carbon dioxide and water (Soltani and Entezari, 2013).



The reduction of MB⁺ by hydroxyl ion produces hydroxyl radicals reacting with other OH[•] to produce H₂O₂. As seen in Eqs. (3) and (4), the peroxide may be said to be very important in the photodegradation process.



An intermediate species of oxygen radical scavenger can react further with MB[•] radical to form O₂^{•-} according to Eq. (5) (Soltani and Entezari, 2013).



Thus, in visible light irradiation, the degradation of MB in basic medium could be preceded via direct reactions of MB with reactive radical species that are formed which can completely degrade MB dye.

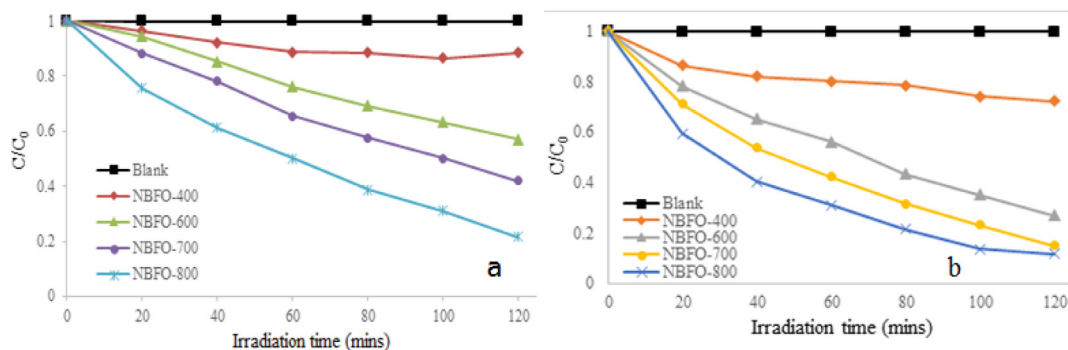


Fig. 11. Photodegradation profile of MB dye solution (a) NBFO 400–800 in absence of peroxide (b) NBFO 400–800 in presence of peroxide.

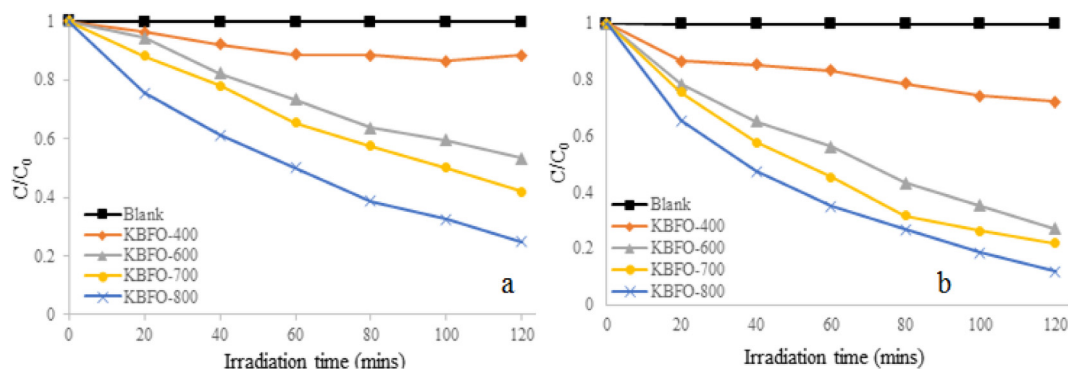


Fig. 12. Photodegradation profile of MB dye solution (a) KBFO 400–800 in absence of peroxide (b) KBFO 400–800 in presence of peroxide.

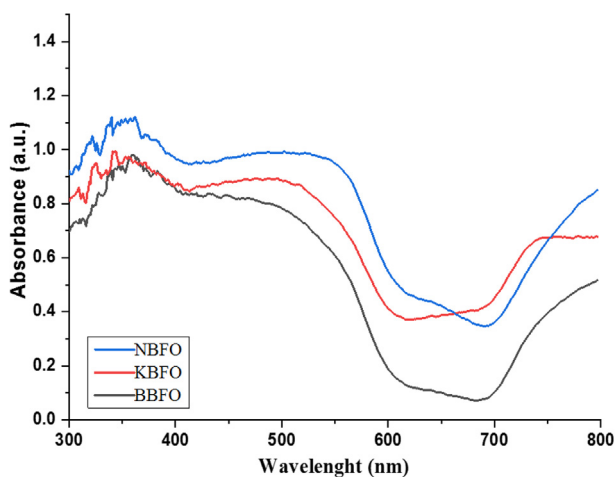


Fig. 13. Uv-vis DRS spectrum of BBFO, NBFO and KBFO nanoparticles.

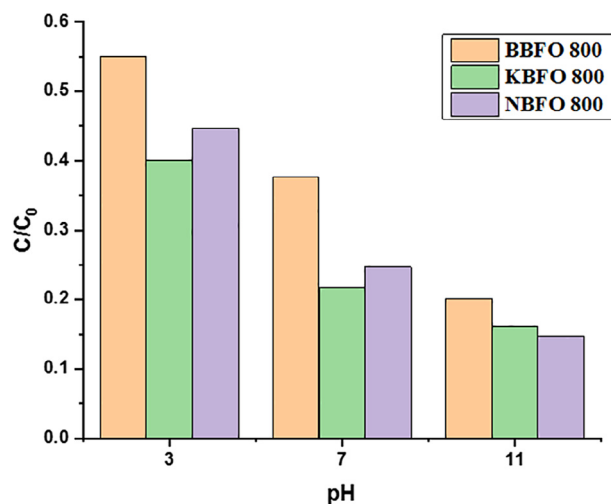


Fig. 14. Effects of pH on MB photodegradation of BBFO, NBFO and KBFO at 800 °C.

3.7. Effect of pH

The concentration of MB dye was kept constant at 10 mg/L throughout the photocatalytic experiments. The effect of pH is one important parameter that influences the photodegradation of organic dye pollutants. The photocatalytic activity of the materials was tested at different pH values of 3, 7 and 11 as shown in Fig. 14. The degradation of pollutants and the effects of pH on the surface charge properties of photocatalyst is variable and controversial (Feng et al., 2004). In acidic medium (pH of 3), the MB photodegradation rate (C/C_0) of all samples drastically decreases and at pH of 11 however, it was interesting to know that the degradation rate of doped and undoped BBFO increases assuming that the highly neg-

ative oxide species and anions influences the surface-charge properties of the photocatalyst. The MB removal efficiency at natural pH 7 and 11 were remarkably great after 120 min and showed improved activity whereas at low pH 3, it showed decreased activity of the photocatalyst. Highest degradation was observed for all samples at pH 11 and a decrease in the rate of degradation for samples at pH 3 is an indication that radicals were not part of the degradation process. The comparison of MB degradation on BFO-doped related materials is shown in Table 2. The various studies indicate that the degradation of organic dyes is hugely affected by the change in pH of the solution from 3 to 11, light source, intensity and the catalyst with suitable dopants concentration.

Table 2
Degradation efficiency of MB metal doped BFO under different conditions.

Study	Concentration MB Catalyst	Volume (ml)	pH	%Degradation $\frac{C_0-C}{C_0} \times 100$	Time (min)	Source of light
This research	10 mg/L BBFO NBFO KBFO BBFO NBFO KBFO BBFO NBFO KBFO	100	3.0	45	100	250 W Xe lamp
			3.0	60	100	
			3.0	56	100	
			7.0	65	120	
			7.0	78	120	
			7.0	75	120	
			11.0	80	90	
			11.0	84	90	
			11.0	85	90	
			Reddy Vanga et al. (2015)	3.2 mg/L La – BFO	350	
Mohan et al. (2014)	1 mg/L Gd – BFO	50	7.0	72	240	Sunlight
Ramadan et al. (2013)	50 μ mol Ca – BFO	50	7.0	100	120	Tungsten 30 mW cm ⁻²

After 100 min at pH value 11, Na and K doping showed a higher degradation efficiency of 84% and 85% respectively than BBFO undoped with 80%. The present study therefore inferred that at high pH, MB was more effectively degraded than BBFO as a result of introduction of metal dopants into the BBFO lattices.

4. Conclusion

In this research, Bi_{0.85-x}M_xBa_{0.15}FeO₃ (M = Na, K and x = 0, 0.1) perovskite-like nanomaterial were synthesized using the sol-gel route in the presence of sodium dodecyl sulfate (SDS), polyethylene glycol and citric acid both as structures – directing and chelating agents. The PXRD pattern of the powders showed a single crystal phase with distorted rhombohedral structure. SEM micrograph of sample powders was in good agreement with the presented XRD results as it shows uniformity in the particle size and morphology which implies that nanoparticles have been formed. The photocatalytic activity of the perovskite nanopowders records very good activity for the photodegradation of MB dye. The effect of pH on MB photodegradation influences the photoactivity of the material with pH 11 having the best degradation for doped samples. The results of this research work further indicate that Na⁺ and K⁺ metal doping were good photocatalyst in peroxide (H₂O₂) leading to improved performance for MB photodegradation under visible light irradiation, with powders annealed at 800 °C being the highest.

References

Ahmed, T., Vorobiev, A., Gevorgian, S., 2012. Growth temperature dependent dielectric properties of BiFeO₃ thin films deposited on silica glass substrates. *Thin Solid Films* 520 (13), 4470–4474. <https://doi.org/10.1016/j.tsf.2012.02.082>.

Abdulkadir, I., Jonnalagadda, S.B., Martincigh, B.S., 2016. Synthesis and effect of annealing temperature on the structural, magnetic and photocatalytic properties of (La_{0.5}Bi_{0.2}Ba_{0.2}Mn_{0.1})FeO_{3-d}. *Mater. Chem. Phys.* 178, 196–203. <https://doi.org/10.1016/j.matchemphys.2016.05.007>.

Bhushan, B., Basumallick, A., Bandopadhyay, S.K., Vasanthacharya, N.Y., Das, D., 2009. Effect of alkaline earth metal doping on thermal, optical, magnetic and dielectric properties of BiFeO₃ nanoparticles. *J. Phys. D: Appl. Phys.* 42, 065004.

Bismibanu, A., 2018. Preparation and characterization of bismuth ferrite nanoparticle using sol-gel method. *Int. J. Res. Appl. Sci. Eng. Technol.* 6 (4), 1767–1770. <https://doi.org/10.22214/ijraset.2018.4299>.

Chaudhuri, A., Mandal, K., 2014. Study of structural, ferromagnetic and ferroelectric properties of nanostructured barium doped Bismuth Ferrite. *J. Magn. Magn. Mater.* 353, 57–64. <https://doi.org/10.1016/j.jmmm.2013.09.049>.

Chang, D.A., Lin, P., Tseng, T.Y., 1995. Optical properties of ZrTiO₄ films grown by radio-frequency magnetron sputtering. *J. Appl. Phys.* 77, 4445–4451.

Chen, X., Zhang, H., Ruan, K., Shi, W., 2012. Annealing effect on the bipolar resistive switching behaviors of BiFeO₃ thin films on LaNiO₃-buffered Si substrates. *J. Alloys Compounds* 529, 108–112. <https://doi.org/10.1016/j.jallcom.2012.03.014>.

El-Desoky, M.M., Ayoua, M.S., Mostafa, M.M., Ahmed, M.A., 2016. Multiferroic properties of nanostructured barium doped bismuth ferrite. *J. Magn. Magn. Mater.* 404, 68–73. <https://doi.org/10.1016/j.jmmm.2015.12.020>.

Fan, T., Chen, C.C., Tang, Z.G., 2016. Hydrothermal synthesis of novel BiFeO₃/BiVO₄ heterojunctions with enhanced photocatalytic activities under visible light irradiation. *RSC Adv.* 6 (12), 9994–10000.

Feng, W., Hong, X., Wang, H., Tao, J., 2004. Photocatalytic property of perovskite bismuth titanate. *Appl. Catal. B Environ.* 52, 109–116. <https://doi.org/10.1016/j.apcatb.2004.04.002>.

Gao, B.F., Chen, X., Yin, K., Dong, S., Ren, Z., Yuan, F., Zou, Z., 2007. Visible-light photocatalytic properties of weak magnetic BiFeO₃ nanoparticles. *Adv. Mater. Banner*, 2889–2892. <https://doi.org/10.1002/adma.200602377>.

Gao, T., Chen, Z., Huang, Q., Niu, F., Huang, X., Qin, L., Huang, Y., 2015. A review: preparation of bismuth ferrite nanoparticles and its applications in visible-light induced photocatalyses. *Rev. Adv. Mater. Sci.* 40 (2), 97–109. <https://doi.org/10.1016/j.aap.2006.06.013>.

Kanhere, P., Chen, Z., 2014. A review on visible light active perovskite-based photocatalysts. *Molecules* 19 (12), 1995–2002. <https://doi.org/10.3390/molecules191219995>.

Kim, J.Y., 2016. Low-temperature hydrothermal synthesis of pure BiFeO₃ nanopowders using triethanolamine and their applications as visible-light. *Photocatalysts* 3755 (24913), 3753–3755. <https://doi.org/10.1111/j.1551-2916.2008.02689.x>.

Li, J., Cai, D., Song, J., Jin, D., Yu, S. and Cheng, J. (2010). Synthesis and photocatalytic property of Ba-doped BiFeO₃ nanoparticles. *Proceedings of the 2010 IEEE International Symposium on the Applications of Ferroelectrics, ISAF 2010, Co-located with the 10th European Conference on the Applications of Polar Dielectrics, ECAPD 2010, 1(1), 3–6. doi: 10.1109/ISAF.2010.5712271*

Mohan, S., Subramanian, B., Bhaumik, I., Gupta, P.K., Jaisankar, S.N., 2014. Nanostructured Bi_(1-x)Gd_(x)FeO₃ – a multiferroic photocatalyst on its sunlight driven photocatalytic activity. *J. R Soc. Chem. Adv.* 4, 16871–16878.

Narayan, S., Mishra, B.G., Shirolkar, M.M., Sen, S., Das, S.R., Janes, D.B., Pradhan, D.K., 2013. Structural, microstructural and magneto-electric properties of single-phase BiFeO₃ nanoceramics prepared by auto-combustion method. *Mater. Chem. Phys.* 141 (1), 423–431. <https://doi.org/10.1016/j.matchemphys.2013.05.040>.

Pandey, S., Misha, S., 2011. Sol-gel derived organic-inorganic hybrid materials: synthesis, characterizations and applications. *J. Sol-Gel Sci. Technol.* 59, 73–94.

Pomogailo, A., 2005. Polymer sol-gel synthesis of hybrid nanocomposites. *Colloid J.* 67, 658–677.

Ramadan, W., Shaikh, P.A., Ebrahim, Sh., Ramadan, A., Hannover, B., Jouen, S., Sauvage, X., Ogale, S., 2013. Highly efficient photocatalysis by BiFeO₃/α(γ)-Fe₂O₃ ferromagnetic nano p/n junctions formed by dopant-induced phase separation. *J. Nanopart. Res.* 15, 1848.

Reddy Vanga, P., Mangalaraja, R.V., Ashok, M., 2015. Structural, magnetic and photocatalytic properties of La and alkaline Co-doped BiFeO₃ nanoparticles. *Mater. Sci. Semicond. Process.* 40, 796–802. <https://doi.org/10.1016/j.mssp.2015.07.078>.

Silva, G.R.O., Santos, J.C., Martinelli, D.M., Pedrosa, A.M.G., de Souza, M.J.B., Melo, D. M.A., 2010. Synthesis and characterization of LaNi_xCo_{1-x}O₃ perovskites via complex precursor methods. *J. Mater. Sci. Appl.* 1, 39–45.

Soltani, T., Entezari, M.H., 2013. Photolysis and photocatalysis of methylene blue by ferrite bismuth nanoparticles under sunlight irradiation. *J. Mole. Catal. A: Chem.* 377 (3), 197–203.

Soltani, T., Entezari, M.H., 2014. Solar-Fenton catalytic degradation of phenolic compounds by impure bismuth ferrite nanoparticles synthesized via ultrasound. *Chem. Eng. J.* 251, 207–216. <https://doi.org/10.1016/j.cej.2014.04.021>.

Soltani, T., Lee, B.K., 2016. Novel and facile synthesis of Ba-doped BiFeO₃ nanoparticles and enhancement of their magnetic and photocatalytic activities for complete degradation of benzene in aqueous solution. *J. Hazard. Mater.* 316. Elsevier B.V. doi: 10.1016/j.jhazmat.2016.03.052.

Vasala, S., Karppinen, P.M., 2014. *SC. Progress in Solid State Chemistry*. Elsevier Ltd. 10.1016/j.progsolidstchem.2014.08.001.

Wang, B., Wang, S., Gong, L., Zhou, Z., 2012. Structural, magnetic and photocatalytic properties of Sr₂-doped BiFeO₃ nanoparticles based on an ultrasonic irradiation assisted self-combustion method. *Ceram. Int.* 38 (8), 6643–6649. <https://doi.org/10.1016/j.ceramint.2012.05.051>.

- Wang, L., Niu, C.G., Wang, Y., Wang, Y., Zeng, G.M., 2016. The synthesis of Ag/AgCl/BiFeO₃ photocatalyst with enhanced visible photocatalytic activity. *Ceram. Int.* 42 (16), 18605–18611. <https://doi.org/10.1016/j.ceramint.2016.08.204>.
- Wang, X., Lin, Y., Zhang, Z.C., Bian, J.Y., 2011. Photocatalytic activities of multiferroic bismuth ferrite nanoparticles prepared by glycol-based sol-gel process. *J. Sol-Gel Sci. Technol.* 60 (1), 1–5. <https://doi.org/10.1007/s10971-011-2542-4>.
- Yao, W.F., Wang, H., Xu, X.H., Yang, X.N., Zhang, Y., Shang, S.X., Wang, M., 2003. Preparation and photocatalytic property of La(Fe) -doped bismuth titanate. *J. Nanosci. Nanotechnol.* 251, 235–239. [https://doi.org/10.1016/S0926-860X\(03\)00378-8](https://doi.org/10.1016/S0926-860X(03)00378-8).
- Zhao, H., Tian, F., Wang, R., Chen, R., 2014. A review on bismuth-related nanomaterials for photocatalysis. *Rev. Adv. Sci. Eng.* 3 (1), 3–27. <https://doi.org/10.1166/rase.2014.1050>.
- Zhang, S.T., Lu, M.H., Wu, D., Chen, Y.F., Ming, N.B., 2005. Larger polarization and weak ferromagnetism in quenched BiFeO₃ ceramics with a distorted rhombohedral crystal structure. *Appl. Phys. Lett.* 87 (262), 907.
- Zhang, T., Shen, Y., Qiu, Y., Liu, Y., Xiong, R., Shi, J., Wei, J., 2017. Facial Synthesis and Photoreaction Mechanism of BiFeO₃/Bi₂Fe₄O₉ Heterojunction Nanofibers. *ACS Sustain Chem. Eng.*, 2–8 <https://doi.org/10.1021/acssuschemeng.6b03138>.